IEEE Access
Multidisciplinary ⋮ Rapid Review ⋮ Open Access Journal

Received 26 February 2023, accepted 17 March 2023, date of publication 22 March 2023, date of current version 29 March 2023.

Digital Object Identifier 10.1109/ACCESS.2023.3260221

RESEARCH ARTICLE

Solution for Self-Interference of NOMA-Based Wireless Optical Communication System in Underwater Turbulence Environment

YANJUN LIANG, HONGXI YIN, LIANYOU JING, (Member, IEEE), XIUYANG JI, AND JIANYING WANG

School of Information and Communication Engineering, Dalian University of Technology, Dalian 116024, China

Corresponding author: Hongxi Yin (hxyin@dlut.edu.cn)

This work was supported in part by the National Natural Science Foundation of China (NSFC) under Grant 61871418 and Grant 61801079, and in part by Science and Technology on Underwater Information and Control Laboratory under Grant 6142218200408.

ABSTRACT Non-orthogonal multiple access (NOMA) is a multiple access technology of great potential and it has superior performance in underwater wireless optical communications (UWOC). In this paper, we investigate the self-interference problem caused by the superimposed transmission of NOMA-based wireless optical communication system in the underwater turbulent environment, and then propose an alternating composite phase shift (ACPS) coding scheme based on constellation optimization, which can effectively eliminate the decoding error caused by the self-interference within the NOMA paired group. To enhance the optimization efficiency of ACPS in the medium- and strong-turbulence environments, we design a golden-section-approach-based power allocation (GSPA) algorithm that minimizes the bit error rate (BER). The simulation results show that the BER of the low-power user within the NOMA paired group can be reduced by up to 3 orders of magnitude in the ACPS-based UWOC-NOMA system compared to the conventional UWOC-NOMA system. In addition, the proposed GSPA algorithm fully takes into account the light-intensity scintillation caused by the ocean turbulence, which not only significantly reduces the average BER of the NOMA system, but also accelerates the convergence rate.

INDEX TERMS Non-orthogonal multiple access, underwater wireless optical communications, alternating composite phase shift, golden-section-approach-based power allocation, bit error rate.

I. INTRODUCTION

Motivated by the fact that there has been a tremendous increase in the demand for the Internet of Underwater Things (IoUTs), the underwater sensor networks are gradually moving towards intensive deployment [1]. While traditional underwater acoustic and electromagnetic communications are no longer able to fully meet the future needs of underwater wireless optical communication (UWOC), regarded as a communication technology that can achieve high capacity, low latency and high flexibility, is considered to be an effective complement to the underwater wireless communications and a significantly improved technology in local area communication performance [2]. The existing optical communication light sources mainly include laser diode (LD) and light emitting diode (LED), etc. Among them, the LD-based optical communication system has the disadvantages of difficult alignment, complex ATP (acquisition, tracking and pointing) implementation and high cost in the dynamic and changing marine environment, while the LED-based optical communication system can effectively control its costs, reduce alignment requirements and mitigate turbulence effects [3], [4], [5], [6]. Thus, LED is frequently chosen to be the light source of the UWOC system. However, the LED-based UWOC system suffers from the problem of insufficient modulation bandwidth. The non-orthogonal multiple access (NOMA) technique has been introduced into the LED-based UWOC system in order to improve the spectrum utilization.

The NOMA is a promising multi-access technology that enables efficient large-scale connectivity and it perfectly

The associate editor coordinating the review of this manuscript and approving it for publication was Jiajia Jiang.

complies the development requirements of IoUTs. There have been sporadic researches that verify the effectiveness of power-division-multiplexing-based (PDM-based) NOMA in the UWOC system application through experiments and simulations [7], [8], [9], [10]. It demonstrated through simulations [7], [8] that NOMA-based UWOC system can increase the system capacity by more than 40% with the same energy consumption compared to the traditional orthogonal-multiple-access-based (OMA-based) system. A 2-user paired NOMA system was designed in [9], which achieved a high-speed transmission of 117.4 Mb/s within 1 m length in the laboratory water tank environment. In [10], the reliability of NOMA technology in the underwater large-scale sensor networks was tested through simulation experiments.

Nevertheless, the study on UWOC-NOMA is still in its infancy, and there are comparatively few studies on interference suppression in the UWOC-NOMA systems. In the NOMA-based communication systems, the superimposed transmission inevitably causes self-interference within the NOMA paired group. This self-interference is mainly reflected in the fact that the bit error judgement for the low-power user will be seriously influenced by the high-power user. In the NOMA-based terrestrial communication systems, the researches on self-interference are mostly focusing on successive interference cancellation (SIC) at the NOMA receiver [11], [12], [13]. In [11], the efficiency of SIC in terms of signal separation for different power allocation scaling factors was discussed. Reference [12] investigated the performance of NOMA systems under ideal SIC and non-ideal SIC conditions in Rayleigh fading channels. Particularly, Reference [13] provided a calculation method for the interference cancellation factor under incomplete SIC, and addressed the effect of the interference factor on the robustness and effectiveness of the NOMA-based optical communication system. The design of power allocation schemes for the NOMA-based UWOC system mostly makes reference to existing terrestrial wireless communication technologies, and the most commonly used are the fixed power allocation algorithm and the distance-based fixed-proportional power allocation algorithm [14], [15], [16]. Both of the two algorithms are easy to be implemented, and however they are not flexible enough to deal with the complex oceanic channel environments, which makes it challenging to achieve the optimal efficiency of the NOMA-based UWOC system. Thus, the existing research achievements cannot be directly applied to the NOMA-based UWOC system due to its distinctive properties, such as the complex and dynamic underwater environments and the distinctive link configurations. Additionally, since seawater is a kind of complex and integrated system the optical signal is not only suffering from the attenuation caused by scattering and absorption, but also the non-uniformity factors such as light intensity scintillation caused by oceanic turbulence. The random perturbations caused by such non-uniformity factors on light propagation further aggravate the self-interference within the NOMA paired user group and lead to an increase in the bit error rate (BER) of NOMA users [17], [18], [19]. To our best knowledge, there have been very few relevant researches on suppressing the self-interference and reducing system BER for the UWOC-NOMA system.

In this paper, an alternating composite phase shift (ACPS) coding scheme based on constellation optimization is proposed for the NOMA-based wireless optical systems in the underwater turbulent environment. Simulation results verify that the scheme can effectively suppress the decoding error caused by the self-interference within the NOMA paired group, and significantly reduce the BER of the low-power user. It is noted that, the ACPS coding scheme can be extended into the multi-user (more than 2) pairing NOMA systems. Furthermore, we design a golden-section-approach-based power allocation (GSPA) algorithm to improve the optimization efficiency of the ACPS scheme for the NOMA-based system in underwater turbulent environments. Compared to the traditional power allocation algorithm, the GSPA algorithm not only diminishes the average BER of the UWOC-NOMA system significantly, but also converges faster.

II. SYSTEM MODELING

A. CHANNEL MODELING

The existing underwater wireless technologies mainly include underwater acoustic, radio frequency (RF) and optical communication techniques. Particularly, compared to underwater acoustic/RF communication, the UWOC suffers from severe attenuation caused by absorption, scattering, turbulence and etc. due to the inherent optical properties of the seawater channel and complex environment. Especially, the random fluctuations in the refractive index of ocean water lead to random fading of the optical signal. Hence, an aggregated channel model is considered here and can be expressed as

$$h = I^2 l \tag{1}$$

where I indicates the fading amplitude incurred by the oceanic turbulence and l represents the path loss induced by the absorption, scattering and optical geometric path between the receiver and the transmitter.

Most studies on the UWOC-NOMA modelled I as a Log-normal distribution to describe the characteristics of oceanic turbulence. However, the Log-Normal distribution is derived from the first-order Rytov approximation. The Rytov variance represents the scintillation index of an infinite plane wave in the case of weak turbulence, it is derived without taking the strongly turbulent situation into consideration at all, implying that the Log-Normal distribution function can only be used as the probabilistic model to analyze the large scale perturbation, i.e., analyzing the channel characteristics of weak turbulence.

On the other hand, the exponential Weibull distribution function was proposed by Barrios and Dios in 2012, which is

proved to be more accurate in the turbulence of diverse intensities with the consideration of aperture averaging in FSO communications [20]. The exponential Weibull distribution function is capable of analyzing both small-scale and large-scale perturbations, and it has excellent fitting properties for turbulent channel properties caused by salinity differences [21]. Meanwhile, the exponential Weibull distribution model properties of turbulence channel caused by salinity differences [21]. Meanwhile, the exponential Weibull distribution model considers the situation when the radius of the beam is much larger than the turbulence scale coherent beams at the receiver end. The light field at the receiving end is divided into collimated components and a small number of multipath components that propagate off the collimated axis. Furthermore, the non-linear relationship between the total light intensity and the independent path light intensities is accurately conveyed by assuming that the light intensity is a weighted sum of several independent light intensity random variables received at the receiver. Therefore, this paper employs the exponential Weibull distribution to model and analyze the oceanic channel applicable to weak and strong turbulences, which can accurately characterize the statistical properties of the optical amplitude fading. The probability density function of I can be given as [22], [23]

$$f(I) = \frac{\delta\beta}{\alpha}\left(\frac{I}{\alpha}\right)^{\beta-1}\left\{\exp\left(-\left(\frac{I}{\alpha}\right)^{\beta}\right)\right\}^{\delta-1} \tag{2}$$

where δ, β are the shape parameters of the exponential Weibull distribution, α denotes the scale parameter. The accuracy of these values has been experimentally verified under ocean turbulence, further enhancing the reliability of the exponential Weibull distribution model. Their expressions are shown below [23]

$$\delta \cong \frac{7.220\sigma_{\text{sci}}^{2/3}}{\Gamma\left(2.487\sigma_{\text{sci}}^{1/3} - 0.104\right)} \tag{3}$$

$$\beta = 1.102\left(\delta\sigma_{\text{sci}}^{2}\right)^{-13/25} + 0.142 \tag{4}$$

$$\alpha = \frac{1}{\delta\Gamma\left(1 + 1/\beta\right) g\left(\delta, \beta\right)} \tag{5}$$

where $\Gamma(\cdot)$ indicates the Gamma function, σ_{sci}^2 denotes the scintillation coefficient, and $g(\cdot, \cdot)$ can be calculated as

$$g\left(\delta, \beta\right) = \sum\nolimits_{m=0}^{\infty} \frac{(-1)^m \Gamma\left(\delta\right)}{m!\left(m+1\right)^{1+1/\beta}\Gamma\left(\delta - m\right)} \tag{6}$$

The path loss of optical signal transmission in the seawater can be expressed in the following form [1], [24], [25]

$$l = \underbrace{\frac{A_{\text{d}}\eta_{\text{t}}\eta_{\text{d}}\cos\theta_0}{2\pi d^2(1-\cos\theta)}}_{\text{geometric loss}}\underbrace{\exp\left[-c\left(\lambda\right)d\right]}_{\text{transmission loss}} \tag{7}$$

where A_{d} is the aperture radius of the optical receiver. η_{t} and η_{d} are the optical efficiencies of the optical transmitter and optical receiver, respectively. θ_0 and θ symbolize the beam divergence angle of the optical transmitter and the inclination angle between the optical transmitter and the optical receiver. d represents the distance between the optical receiver and the optical transmitter. $c(\lambda)$ stands for the attenuation coefficient, $c(\lambda) = a(\lambda) + b(\lambda)$, $a(\lambda)$ and $b(\lambda)$ denote the absorption coefficient and the scattering coefficient, respectively. The typical values of seawater for $c(\lambda)$ can be referred to in [6].

B. NOISE MODELING

Generally, there exist various types of noises that disturb UOWC, such as quantum noise, dark current noise, thermal noise, solar radiation background noise and so forth. Most of the previous works treat the underwater noise as a constant, which is not entirely consistent with reality. For the underwater environment, solar radiation background noise varies significantly with the water quality and depth of seawater and thus affecting the communication system performance to varying degrees. The variance of solar radiation noise for a horizontal link can be given as [26]

$$\sigma_{\text{sol}}^2 = 2.9ERA_{\text{d}}\theta_{\text{f}}^2F\Delta\lambda\exp\left[-c\left(\lambda\right)d_{\text{p}}\right] \tag{8}$$

where E is the downlink irradiance. R signifies the reflection ratio of seawater to spectral irradiance. θ_{f} represents the field of view of the optical receiver. F indicates the optical filter transmissivity. $\Delta\lambda$ is the optical filter bandwidth, and d_{p} is the seawater depth.

The analysis of quantum noise necessitates taking into account both sunlight and received signal light. Hence, the variance of quantum noise can be derived as [26]

$$\sigma_{\text{shot}}^2 = 2mg\eta_{\text{d}}\left[lP_{\text{t}} + \sigma_{\text{sol}}^2\right]\Delta\lambda\left[k_{\text{A}}g + \left(1-k_{\text{A}}\right)\left(2 - \frac{1}{g}\right)\right] \tag{9}$$

where m denotes the modulation index. g indicates the APD avalanche gain factor. P_{t} is the total transmitted optical power. k_{A} signifies the ionization index.

The noise component in the UWOC system can all be approximately modelled as additive white Gaussian noise (AWGN). The sum variance of other noises, such as thermal noise and dark current noise, is assumed to be σ_{oth}^2. The variance of the total noise can be computed by

$$\sigma_0^2 = \sigma_{\text{sol}}^2 + \sigma_{\text{shot}}^2 + \sigma_{\text{oth}}^2 \tag{10}$$

C. UWOC-NOMA SYSTEM MODELING

We consider a 2-user paired NOMA system for UWOC depicted in Fig. 1. The input binary data information completes the quadrature amplitude modulation (QAM) constellation mapping based on Gray coding, and then $(N/2)$-1 parallel frequency domain signal is obtained by serial/parallel conversion. The real-valued signal is generated by Hermitian symmetry, and the frequency domain signal with conjugate symmetry is input to the inverse fast Fourier transformation (IFFT) module to obtain the user's time domain signal.

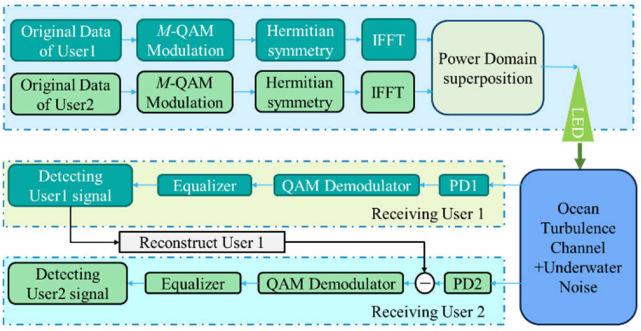

FIGURE 1. Schematic diagram for UWOC-NOMA system.

Finally, according to the superposition principle of NOMA, the transmitted superimposed signal can be given as

$$x = a_1 P_t x_1 + a_2 P_t x_2 \tag{11}$$

where a_1 and a_2 denote the power allocation coefficients of User 1 and User 2, respectively. x_1 and x_2 are the transmitted signals of User 1 and User 2 respectively. The aggregated channel quality of User 1 is assumed worse than that of User 2 here.

Correspondingly, the signal received by the i^{th} receiving user can be expressed as

$$y_i = \Re h_i x + n_i \, (i = 1, 2) \tag{12}$$

where $\Re$ is the responsivity of the photodetector. h_i and n_i are the aggregated channel loss and the noise between the transmitter and the i^{th} receiver.

III. ANALYSIS AND OPTIMIZATION OF SELF-INTERFERENCE CAUSED BY THE CONSTELLATION

Differing from that of the orthogonal multiple access (OMA) system, the BER analysis of the NOMA-based system requires taking into account the decomposition of superimposed signal and the BER propagation with a NOMA paired group. In this section, we analyze the BER of the NOMA-based UWOC system and propose an optimized coding scheme caused by the constellation diagram for the non-Gray characteristics of superimposed NOMA signals.

4-QAM is employed here. The mapping symbol sequence for the signal of the i^{th} user on the constellation diagram can be given as

$$C_m^{i,n}\Big|_{n=0}^{N-1} = \left[A_m^{i,n} + jZ_m^{i,n}\right]\Big|_{n=0}^{N-1} \tag{13}$$

where $C_m^{i,n}$ denotes the m^{th} constellation mapping symbol of the i^{th} user on the n^{th} subcarrier. N is the number of subcarriers. $A_m^{i,n}$ and $Z_m^{i,n}$ are the real part and the imaginary part of $C_m^{i,n}$ respectively.

The constellations of a NOMA paired group are shown in Fig. 2. Fig. 2(a) illustrates the constellation mapping of User 1, which corresponds to the high-power user in the NOMA paired group. Fig. 2(b) illustrates the constellation mapping of User 2, which corresponds to the low-power user.

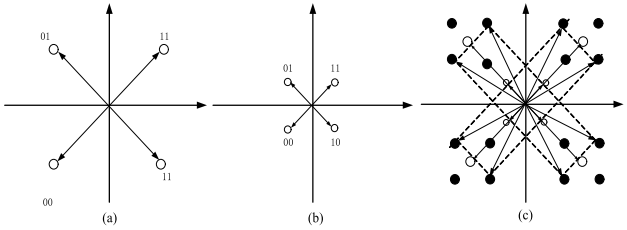

FIGURE 2. Constellation analysis model for (a) constellation diagram of User 1, (b) constellation diagram of User 2, (c) superposition process of NOMA signal.

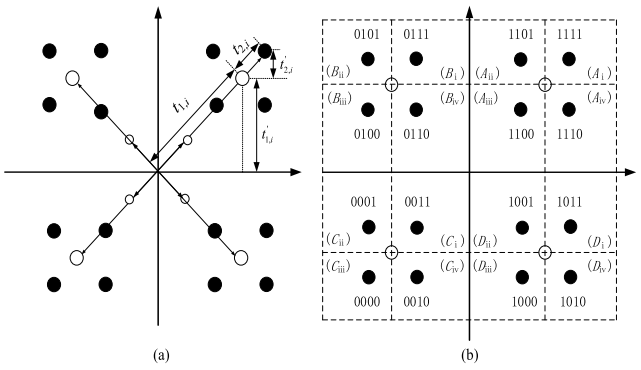

FIGURE 3. BER analysis model of NOMA for: (a) distance between the constellation points, (b) BER judgement regions.

The superposition of User 1 and User 2 can be regarded as the summation between the vectors in Fig. 2(a) and Fig. 2(b), and the detailed superposition process is depicted in Fig. 2(c). The superposition of two 4-QAM signals yields 16 new constellation points. The format of each new constellation point is (a_1, a_2, b_1, b_2), where (a_1, a_2) belongs to User 1 and (b_1, b_2) belongs to User 2.

A. BER ANALYSIS OF UWOC-NOMA SYSTEM

According to the SIC principle, the receiver decodes the high-power signal first, subtract it from the superimposed signal, and isolates the low-power signal from the residue. For the constellation diagram, the signal decomposition can be regarded as the vectors in Fig. 2(c) being decomposed into the vectors in Fig. 2(a) and Fig. 2(b). Fig. 3(b) illustrates the judgement region for BER of the NOMA signal. To facilitate the analysis, each quadrant is divided into four sub-quadrants according to the regions of extended NOMA constellation points as shown in Fig. 3(b). For example, the first quadrant is split up into A_{i}, A_{ii}, A_{iii} and A_{iv}.

As can be seen in Fig. 3(b), User 1 in the same quadrant has the same decision result. The signal of User 1 is incorrectly demodulated only if the constellation point moves to the adjacent region of another quadrant. For the signal of User 2, the demodulations performed in the same sub-quadrant of four quadrants have the same results. For example, when the signals are mapped in the region of A_{i}, B_{i}, C_{i}, D_{i}, the signals have the same decision results. Otherwise, errors are occurring for the demodulation of User 2.

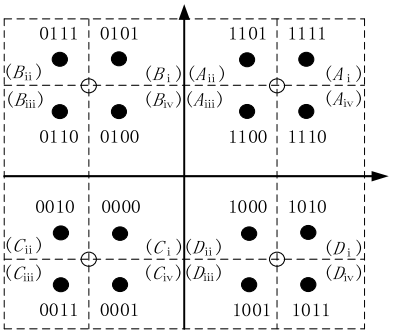

FIGURE 4. Optimized constellation with ACPS.

It can be observed from Fig. 3(a) that the minimum distances between the receiver constellation points of the two users are respectively [27]

$$t_{1,i} = \frac{B}{2}\sqrt{\frac{3}{2\,(4-1)}\frac{a_1 P_t h_i^2}{n_i}} \tag{14}$$

$$t_{2,i} = \frac{B}{2}\sqrt{\frac{3}{2\,(4-1)}\frac{a_2 P_t h_i^2}{n_i}} \tag{15}$$

Based on the analysis above, the BER of User 1 can be calculated by

$$P_{\mathrm{U1,O}} = \frac{1}{2}\left[\Theta\left(2\frac{t'_{1,1}+t'_{2,1}}{B}\right)+\Theta\left(2\frac{t'_{1,1}-t'_{2,1}}{B}\right)\right] \tag{16}$$

The solution of Θ function in (16) can be referred to in Appendix A.

When deriving the BER of User 2, it is required to take into account the demodulation result of User 1. Thus, the BER of User 2 can be solved as

$$P_{\mathrm{U2,O}} = \sum_{i=1}^{2}\sum_{j=0}^{1}\sum_{bs=00}^{11} P_{b_i=j|(a_1a_2)=bs} \tag{17}$$

Details of proof are elaborated in Appendix B.

B. ALTERNATING COMPOSITE PHASE SHIFT CODING SCHEME BASED ON CONSTELLATION OPTIMIZATION

It can be obviously told from Fig. 3(b) that although the original modulation symbols are mapped to the bit patterns by using grey code, the superimposed signals do not satisfy the grey code rule. To avoid the situation that the demodulation error of User 2 will lead to the demodulation error of User 1, the location of User 2 in the constellation requires reconfiguration in order to optimize the distribution of the superimposed signals in the constellation. The core idea of this optimized coding scheme is to achieve a grey distribution for the joint constellation. Different phase shift factors will be inserted into the low-power user in accordance with the location of the constellation points of the high-power user in the joint constellation. The specific coding scheme can be accomplished by **Algorithm 1.**

Fig. 4 shows the BER judgment region for the two paired NOMA users with ACPS coding scheme. Compared to that of Fig. 3(b), the distribution of the BER judgment region for User 2 is symmetrical in accordance with the decision threshold for User 1 in Fig. 4. Thus, the demodulation error of User 1 will be hardly causing the demodulation error of User 2. According to the analysis above, the BER judgment region of User 1 remains unchanged, and thus the BER of User 1 can still be calculated by (16). It is noted that the interference cancellation method based on the fixed sorting of power-graded magnitudes is employed in this paper for the sake of interference cancellation efficiency. Based on the above, the stronger user is User 2 and the weaker user is User 1 in the proposed UWOC-NOMA system. The basic idea of SIC is that the stronger user will be decoded, treating the weaker user as an interferer. Then, User 1 can be decoded with the benefit of the signal of User 2 having already been removed. Thus, the effect of the demodulation error of User 1 has hardly an effect on the demodulation of User 2. In reality, the impact of noise and interference on the BER is negligible when they exceed $2t'_{1,1}$ [27]. The BER of User 2 can be given as

$$P_{\mathrm{U2}} = \Theta\left(\frac{2t'_{2,2}}{B}\right) + \frac{1}{2}\sum_{i=1}^{2}\sum_{j=1}^{2}(-1)^i\Theta\left(\frac{jt'_{1,2}+(-1)^{i+j}t'_{2,2}}{B}\right). \tag{18}$$

Algorithm 1 Superposition Coding of Alternating Composite Phase Shifts

Step 1: Produce the symbol sequence.

$X_1 : C_m^{1,n}\big|_{n=0}^{N-1} = \left[A_m^{1,n} + jZ_m^{1,n}\right]\big|_{n=0}^{N-1}$

$X_2 : C_m^{2,n}\big|_{n=0}^{N-1} = \left[A_m^{2,n} + jZ_m^{2,n}\right]\big|_{n=0}^{N-1}$

Step 2: Extract the real and imaginary parts of the signal of User 2

Step 3: Divide the real and imaginary parts of the signal of User 2 into two paths

Step 4: Achieve the phase shift alternately.

if $A_m^{1,n} < 0 \& Z_m^{1,n} > 0$

  $A_m^{2,n} = -A_m^{2,n}$

else if $A_m^{1,n} < 0 \& Z_m^{1,n} < 0$

  $A_m^{2,n} = -A_m^{2,n}, Z_m^{2,n} = -Z_m^{2,n}$

else if $A_m^{1,n} > 0 \& Z_m^{1,n} < 0$

  $Z_m^{2,n} = -Z_m^{2,n}$

Step 5: Generate the new signal

$$x_1 = \frac{1}{\sqrt{N}}\sum_{n=0}^{N-1}\sum_{m=0}^{M-1}\left(A_m^{1,n} + jZ_m^{1,n}\right)e^{\frac{2n\pi j}{N}},$$

$$x_2 = \frac{1}{\sqrt{N}}\sum_{n=0}^{N-1}\sum_{m=0}^{M-1}\left(A_m^{2,n} + jZ_m^{2,n}\right)e^{\frac{2n\pi j}{N}}$$

Step 6: Signal superposition

$x = a_1x_1 + a_2x_2$

Note that this proposed ACPS coding scheme is also available for the multi-user paired NOMA system (the paired users

are more than 2). It can be accomplished by treating the superimposed signals as the low power user in Step 2 and the newly added user is regarded as the high power user in Step 1. Then, repeat Step 3 - Step 6.

IV. POWER ALLOCATION ALGORITHM BASED ON THE BER OPTIMIZATION

A. GOLDEN-SECTION-APPROACH POWER ALLOCATION ALGORITHM

Based on the previous study, the BER of the low power user is much higher than that of the high power user in the NOMA system. Therefore, the critical concern is to reduce the BER of the a NOMA-based system. In this sub-section, the optimization objective is set to minimize the BER of User 2, under the premise of consuming a certain amount of transmitted power. The power allocation problem can be formulated as

$$\begin{aligned} &\min \quad P_{\mathrm{U2}} && \text{(19-a)}\\ &\text{subject to} \quad a_1 > a_2 > 0 && \text{(19-b)}\\ &\qquad\qquad a_1 + a_2 \le 1 && \text{(19-c)} \end{aligned}$$

It is a challenging task to solve the problem in (19) since it contains some Θ-functions derived from the integration of multiple Q-functions. A high complexity transcendental equation is required to be solved in order to obtain the optimal power allocation factor from (19). To solve it, we will first investigate its concave-convexity property. The bordered Hessian matrix of P_{U2} with respect to a_1, a_2, can be expressed as

$$H = \begin{pmatrix} 0 & \frac{\partial P_{\mathrm{U2}}}{\partial a_1} & \frac{\partial P_{\mathrm{U2}}}{\partial a_2} \\ \frac{\partial P_{\mathrm{U2}}}{\partial a_1} & \frac{\partial^2 P_{\mathrm{U2}}}{\partial a_1^2} & \frac{\partial^2 P_{\mathrm{U2}}}{\partial a_1 \partial a_2} \\ \frac{\partial P_{\mathrm{U2}}}{\partial a_2} & \frac{\partial^2 P_{\mathrm{U2}}}{\partial a_1 \partial a_2} & \frac{\partial^2 P_{\mathrm{U2}}}{\partial a_2^2} \end{pmatrix} \tag{20}$$

After mathematical calculation, we can get det($\mathbf{H}$)>0, det ($\mathbf{H}_2$) <0. The detailed proof can be found in **Appendix C**. P_{U2} is proved to be strictly convex with respect to a_1, a_2. Thus, the optimization problem in (19) is a strictly convex problem and its solution will provide the globally optimal result. To obtain the optimal solution, we propose a golden-section-approach power allocation algorithm (GSPA). The Lagrangian function for this optimization problem can be formulated as

$$L\left(a_1, a_2, l_1, l_2, l_3\right) = P_{\mathrm{U2}} + l_1\left(a_1 + a_2 - 1\right) - l_2 a_1 - l_3 a_2 \tag{21}$$

According to the Karush-Kuhn-Tucker (KKT) conditions, a_1, a_2, l_1, l_2, l_3, should satisfy the following equations,

$$\begin{aligned} &\frac{\partial L}{\partial a_1} = \frac{\partial P_{\mathrm{U2}}}{\partial a_1} + l_1 - l_2 = 0 && \text{(22-a)}\\ &\frac{\partial L}{\partial a_2} = \frac{\partial P_{\mathrm{U2}}}{\partial a_2} + l_1 - l_3 = 0 && \text{(22-b)}\\ &l_1\left(a_1 + a_2 - 1\right) = 0 && \text{(22-c)}\\ &l_2 a_1 = 0, l_3 a_2 = 0 && \text{(22-d)}\\ &a_1 > 0, a_2 > 0, l_1 \ge 0, l_2 \ge 0, l_3 \ge 0 && \text{(22-e)} \end{aligned}$$

It can be concluded from (22-d) and (22-e) that l_2 =0, l_3 =0. The other parameters, such as a_1, a_2, l_1, can be obtained by solving (22-a)-(22-c). In addition, the optimization problem can be solved optimally only when $a_1 + a_2$ =1. Considering the algorithm complexity, a_2 =1-a_1 is substituted into (21). Although the solution of l_1 cannot be directly derived by (22-b), the definition domain can be obtained from (22-a) and (C.1), (C.3) in **Appendix C**. l_1 should satisfy the following condition on condition that l_1 is a real number,

$$\begin{aligned} l_1 \le \frac{1}{2\sqrt{a_2}} \exp\left(3t_1^2 - 6t_1 t_2\right)\left[\frac{2}{\left(2t_1 - t_2\right)^2} - \frac{1}{\left(t_1 + t_2\right)^2}\right] \\ \times \left[1 - Q\left(\frac{\delta\beta - \beta}{2t_2 + t_1}\right)\right] \end{aligned} \tag{23}$$

In addition, owing to that $(\delta\beta - \beta)/(2t_2 + t_1) > 0$, $0 < Q\left[(\delta\beta - \beta)/(2t_2 + t_1)\right] < 0.5$, (23) can be further simplified as

$$l_1 \le \frac{1}{4\sqrt{a_2}} \exp\left(3t_1^2 - 6t_1 t_2\right)\left[\frac{2}{\left(2t_1 - t_2\right)^2} - \frac{1}{\left(t_1 + t_2\right)^2}\right] \tag{24}$$

According to the power allocation principle of NOMA, the search interval of a_1 is (0.5, 1), and the iterative formulas of

Algorithm 2 Power Allocation Algorithm Based on Golden Section Approach

Initializetotal transmitted power P_{t}, a small number for the accuracy of the algorithm bh, the iteration $k = 0$

Step 1: Define the searching space of $a1$ and $l1$ and calculate the initial value

min $(a1) = 0$, max $(a1) = 0.5$

min $(l1) = 0$, max $(l1)$ can be calculated by (24)

$$L_l = L\left(a_{1,l}^{(0)}, l_{1,l}^{(0)}\right)$$
$$L_r = L\left(a_{1,r}^{(0)}, l_{1,r}^{(0)}\right)$$

Step 2: Power Allocation

while $\left|\left(a_{1,l}^{(k)}, l_{1,l}^{(k)}\right) - \left(a_{1,r}^{(k)}, l_{1,r}^{(k)}\right)\right| \ge \delta_{\mathrm{m}}$

$k = k + 1$

if $L\left(a_{1,l}^{(k)}, l_{1,l}^{(k)}\right) > L\left(a_{1,r}^{(k)}, l_{1,r}^{(k)}\right)$

$\left(b_1^{(k+1)}, b_2^{(k+1)}\right) = \left(b_1^{(k)}, b_2^{(k)}\right), \left(c_1^{(k+1)}, c_2^{(k+1)}\right) = \left(a_{1,r}^{(k)}, l_{1,r}^{(k)}\right)$

$$L_r = L_l$$

$$\left(a_{1,l}^{(k+1)}, l_{1,l}^{(k+1)}\right) = \left(b_1^{(k+1)}, b_2^{(k+1)}\right) + 0.382\left[\left(c_1^{(k+1)}, c_2^{(k+1)}\right) - \left(b_1^{(k+1)}, b_2^{(k+1)}\right)\right]$$

$$L_l = L\left(a_{1,+}^{(k+1)}, l_{1,l}^{(k+1)}\right)$$

else

$\left(b_1^{(k+1)}, b_2^{(k+1)}\right) = \left(a_{1,l}^{(k)}, l_{1,l}^{(k)}\right), \left(c_1^{(k+1)}, c_2^{(k+1)}\right) = \left(c_1^{(k)}, c_2^{(k)}\right)$

$$L_l = L_r$$

$$\left(a_{1,r}^{(k+1)}, l_{1,r}^{(k+1)}\right) = \left(b_1^{(k+1)}, b_2^{(k+1)}\right) + 0.612\left[\left(c_1^{(k+1)}, c_2^{(k+1)}\right) - \left(b_1^{(k+1)}, b_2^{(k+1)}\right)\right]$$

$$L_r = L\left(a_{1,r}^{(k+1)}, l_{1,r}^{(k+1)}\right)$$

end if

$$L_{\min} = L\left(\frac{a_{1,l}^{(k)} + a_{1,r}^{(k)}}{2}, \frac{l_{1,l}^{(k)} + l_{1,r}^{(k)}}{2}\right)$$

end while

return the power allocation coefficient $a\ (a^{00} + a^{(k)})/2$, $a_2 = 1 - a_1$.

the search points are

$$\left(a_{1,l}^{(k)}, l_{1,l}^{(k)}\right) = \left(b_1^{(k)}, b_2^{(k)}\right) + 0.382\left[\left(c_1^{(k)}, c_2^{(k)}\right) - \left(b_1^{(k)}, b_2^{(k)}\right)\right] \quad (25\text{-a})$$

$$\left(a_{1,r}^{(k)}, l_{1,r}^{(k)}\right) = \left(b_1^{(k)}, b_2^{(k)}\right) + 0.618\left[\left(c_1^{(k)}, c_2^{(k)}\right) - \left(b_1^{(k)}, b_2^{(k)}\right)\right] \quad (25\text{-b})$$

Eq. (25-a) represents the iterative formula in the left search region. $b_{1,l}^{(k)}$ and $c_{1,l}^{(k)}$ are the search interval of a_1 in the left search region in the k^{th} iteration. $b_{2,l}^{(k)}$ and $c_{2,l}^{(k)}$ are the search interval of l_1 in the left search region in the k^{th} iteration. Correspondingly, (25-b) denotes the iteration formula in the right search region. The GSPA algorithm is designed as shown in **Algorithm 2**.

It is noted that the proposed GSPA algorithm can be available for the multi-user paired NOMA system. As the paired users are more than 2, the users are grouped as strong users and weak users based on the channel quality. The two weakest users of them primarily perform the power allocation with the GSPA algorithm to generate an independent composite signal. Then the GSPS algorithm is applied in the same way to distribute the power coefficient to the superimposed signal and the signal of stronger users one by one.

B. ANALYSIS OF ALGORITHM COMPLEXITY

To evaluate the algorithm complexity of the proposed golden-section-approach power allocation algorithm, two other most commonly used power allocation schemes that are the fixed power allocation algorithm (FPA) and the distance-based fixed-proportional power allocation algorithm (DFPA), are given to solve the problem in (19).

The FPA algorithm can solve the problem in (19) with a straightforward nested loop, and the optimized results of BER can be resolved using straightforward multiplication and addition operations. Since the DFPA algorithm is likewise a kind of fixed power allocation algorithm, the DFPA algorithm is cyclically nested in the same way as the FPA algorithm. And the ordering of user operations is required in DFPA. Considering that the DFPA and FPA algorithms are iterative algorithms with no search direction, it is essentially an omnidirectional search scheme that relies on the step factor. In contrast, the GSPA algorithm can optimize the search direction and step factor solution process by constructing bordered Hessian matrix. Thus, the problem size of GSPA in a single iteration is small and the algorithm complexity is proportional to the number of iterations and the initialized population size. The problem size of a single mathematical calculation is set to 1 here. To summarize, the complexity statistics for the three algorithms are shown in Table 1, where M is the number of paired user in a NOMA group, τ is the step factor, and K is the maximum number of iterations.

TABLE 1. Comparison of algorithm complexity.

Algorithm	Time Complexity	Problem Size
FPA	$O(s_{\max})$	$255M/\tau$
DFPA	$O(s_{\max})$	$511M/\tau$
GSPA	$O(s_{\max}^2)$	$127MK$

TABLE 2. Simulation parameters.

Parameters	Values	Parameters	Values
A_d	0.01m^2	θ_0	30^o
η_t	0.9	θ_f	40^o
η_d	0.9	E	1440W/m^2
$c(\lambda)$	0.1514m^{-1}	$\Delta\lambda$	30nm
R	1.25%	F	0.95
m	4	k_A	0.04
g	20	σ_{oth}^2	10^{-7}A/Hz

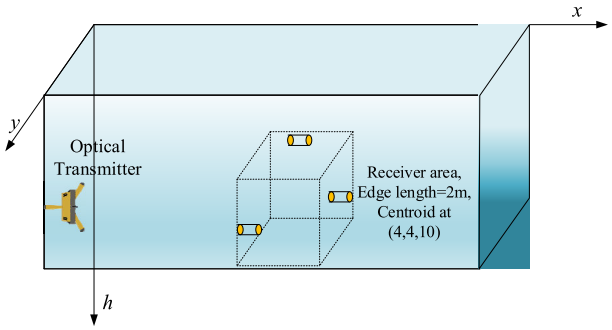

FIGURE 5. Simulation scenarios for the UWOC-NOMA system.

V. PERFORMANCE EVALUATIONS

In this section, we present comprehensive simulation studies to verify the performance of the proposed ACPS coding scheme and the GSPA algorithm. The simulation parameters used in this paper are shown in Table 2.

The simulation scenarios for the UWOC-NOMA system are designed as shown in Fig. 5. There are 3 receiving users deployed in the cube area with edge lengths of 3 m, which are named User 1, User 2 and User 3 in order according to the transmission distance with the optical transmitter from far to near. These three receiving users are at (5, 4, 10), (4, 0, 9) and (3, 5, 10), respectively. The centroid of the cube area is at (4, 4, 10), and the optical transmitter is at (0, 2, 10). Assume that $S_{M,K}$ stands for the NOMA paired group among User M and User K.

A. PERFORMANCE EVALUATIONS OF THE PROPOSED ALTERNATING COMPOSITE PHASE SHIFT CODING SCHEME

According to the theoretical analysis of the BER of UWOC-NOMA system in subsection II-A, it is known that the BER performance of UWOC-NOMA system has a great relation to the power allocation. To assess the performance of the proposed alternating composite phase shift coding

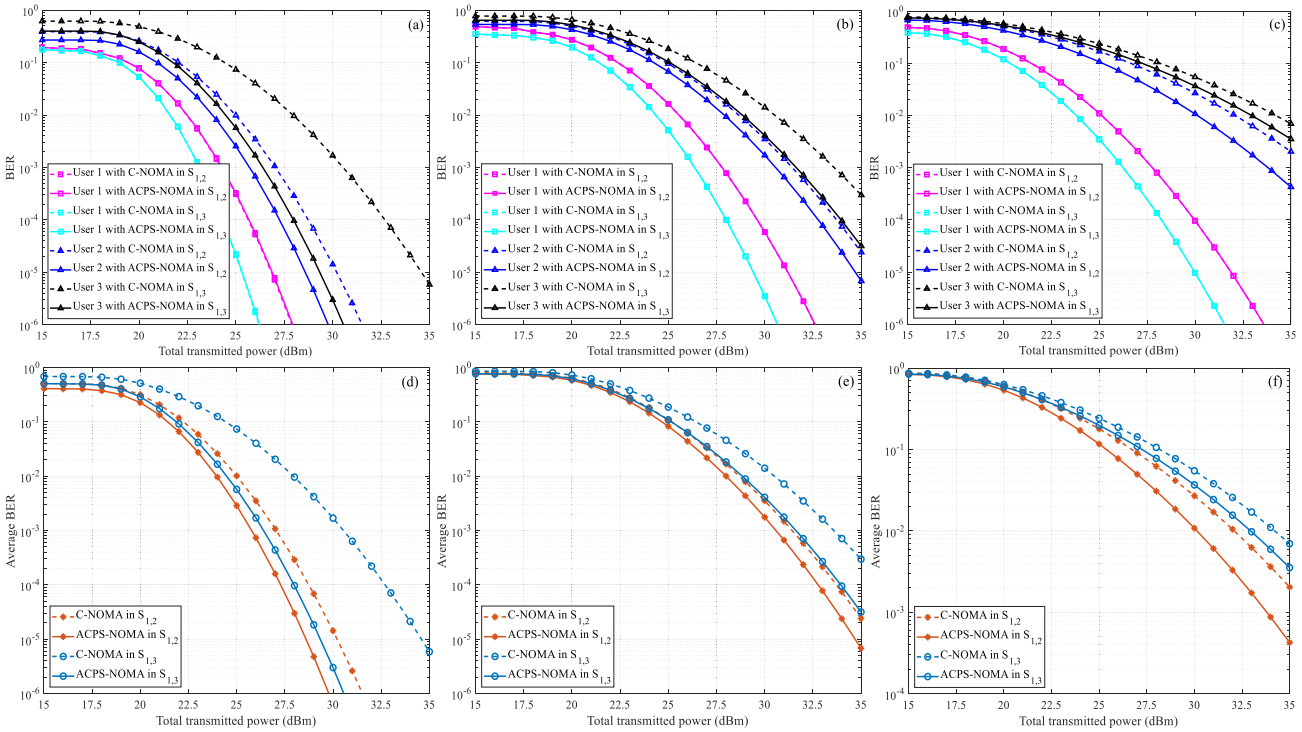

FIGURE 6. Comparisons of 2-user paired C-NOMA and ACPS-NOMA under underwater turbulence channel for (a) and (d): $\sigma_{\text{sci}}^2 = 0.1$, (b) and (e): $\sigma_{\text{sci}}^2 = 0.5$, (c) and (f): $\sigma_{\text{sci}}^2 = 1.0$.

scheme (denoted as ACPS-NOMA) in a fair way, we conduct 10 repeated simulation experiments to obtain the optimal power allocation results under the same signal-to-noise ratio (SNR) regime. The fixed power allocation (FPA) algorithm and the bisection method are adopted to obtain the power allocation coefficient. The conventional NOMA (denoted as C-NOMA) coding scheme is given as a contrast.

The simulation results are shown in Fig. 6. It can be seen that the ACPS-NOMA has essentially no effect on the performance of the high-power user, i.e., User 1 in the NOMA paired group. However, the optimization for the BER of the low power users, i.e., User 2 and User 3 in the NOMA paired group, is particularly effective. Moreover, as Fig. 6(a) and Fig. 6(d) illustrate that User 3 in $S_{1,3}$ with the proposed ACPS-NOMA obviously outperforms User 2 in $S_{1,2}$ in the weak turbulence environment. It is due to the fact that the channel quality difference of paired users in $S_{1,3}$ is much larger than that of $S_{1,2}$, causing that the power allocation coefficient difference in $S_{1,3}$ is much larger than that of $S_{1,2}$. Thus, the signal demodulation of User 3 has a greater chance to be affected by User 1 with C-NOMA coding scheme in $S_{1,3}$. This verifies that ACPA-NOMA can particularly reduce the decoding error caused by the interference of the high power user within a NOMA group. However, the results in Fig. 6(b) and Fig. 6(c) show that the BER optimization efficiency of the proposed ACPS-NOMA scheme has a significant degradation in the strong turbulence environment. When $\sigma_{\text{sci}}^2 = 0.1$ and $P_{\text{t}} = 27.5$dBm, the ACPS-NOMA reduces the BER of User 2 by 1 order of magnitude in $S_{1,2}$, and the BER

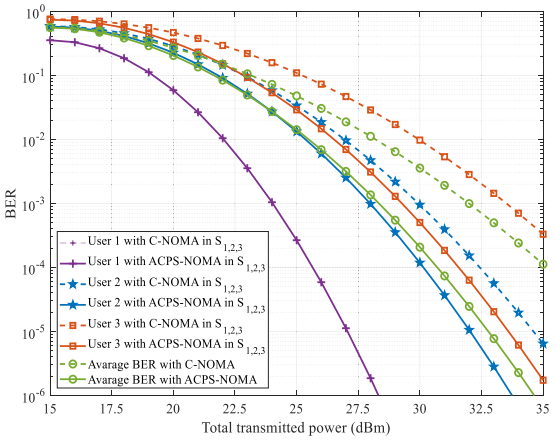

FIGURE 7. BER of three schemes with two 2-user paired NOMA scenarios for (a) $\sigma_{\text{sci}}^2 = 0.1$, (b) $\sigma_{\text{sci}}^2 = 0.5$, (c) $\sigma_{\text{sci}}^2 = 1.0$.

of User 3 is reduced by nearly 2 orders of magnitude in $S_{1,2}$. Meanwhile, at the same transmit power, when $\sigma_{\text{sci}}^2 = 1.0$, the BER of User 2 in $S_{1,2}$ with the ACPS-NOMA scheme is reduced by less than 50%, and the BER of User 3 in $S_{1,3}$ is reduced by less than 30%. This is owing to the fact that in the strong turbulent channel, the decoding error propagated from the high power user will be relatively decreased, and thus, the optimization efficiency of the ACPS for low-power users is reduced.

Fig. 7 shows the BER performance comparisons between the C-NOMA system and the ACPS-NOMA system in the 3-user paired scenario at $\sigma_{\text{sci}}^2 = 0.1$. It can be found that

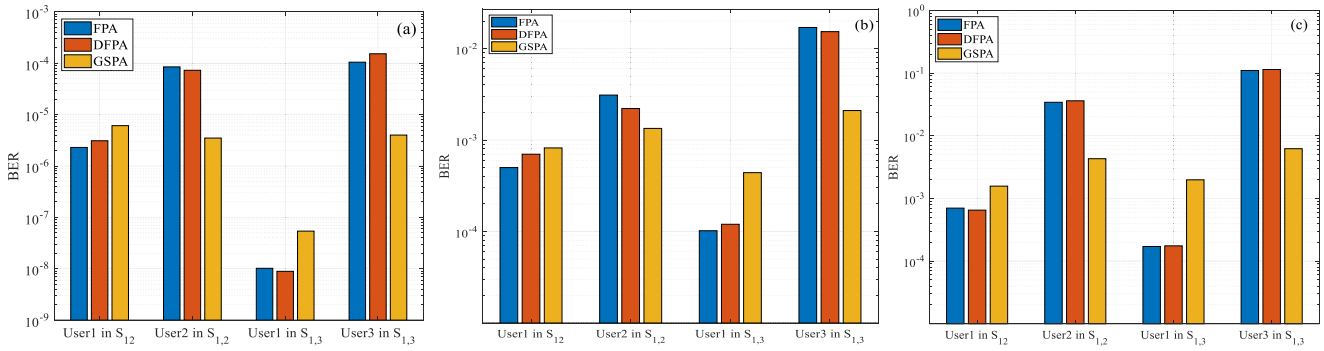

FIGURE 8. BER of three schemes with two 2-user paired NOMA scenarios for (a) $\sigma_{\text{sci}}^2 = 0.1$, (b) $\sigma_{\text{sci}}^2 = 0.5$, (c) $\sigma_{\text{sci}}^2 = 1.0$.

similar to that of 2-user paired NOMA, the ACPS-NOMA scheme has basically no effect on the BER performance of User 1, but the effect on User 2 and User 3 is evident. Moreover, the optimization efficiency of the proposed ACPS-NOMA for the BER of User 2 and User 3 is enhanced as the transmitted power increases. The simulation results verify the effectiveness of the proposed ACPS coding scheme for the multiple-user paired UWOC-NOMA system.

B. PERFORMANCE EVALUATIONS OF THE PROPOSED GOLDEN-SECTION- APPROACH POWER ALLOCATION ALGORITHM

To evaluate the performance of the proposed golden-section-approach power allocation algorithm (denoted as the GSPA), we present two other schemes as contrasts, which are summarized as follows.

i) Fixed power allocation algorithm (denoted as the FPA) The FPA algorithm starts with a power allocation coefficient of 0, whose per update step size is 0.01, and 10 times of simulations are performed to obtain a relative optimal result [14], [15].

ii) Distance-based fixed-proportional power allocation algorithm (denoted as DFPA) [16].

The DFPA algorithm assigns the transmitted power for users according to the Euclidean distance between the receiving user and the optical transmitter. For the signal of user i, the power allocation factor is $d_i \Big/ \sum_{n=1}^{N} d_n$, where d_i denotes the Euclidean distance between the receiving user i and the transmitter, and N denotes the number of paired users within a NOMA group.

The proposed GSPA and the above two algorithms are evaluated in $S_{1,2}$ and $S_{1,3}$, respectively, the results obtained are shown in Fig. 8. In any simulation scenario, the BER of high power users with the GSPA algorithm has a minor increase compared to those of the FPA and the DFPA algorithms, while the BER of low power users with the GSPA is reduced substantially. With the increase of turbulence intensity, the optimization efficiency of the GSPA for the BER of low power users is significantly enhanced. This is due to the fact that the existing power allocation schemes, both the FPA and the DFPA algorithms, merely take into account the attenuation characteristics of the ocean optical channel and ignore the light intensity scintillation caused by diverse turbulences. On the one hand, this will cause the allocation of less power to low-power users and more power to high-power users within the paired user group of the UWOC-NOMA system, which boosts the unfairness of the system, and thus leads to the increase of BER for low-power users. On the other hand, the BER results obtained by the FPA algorithm and the DFPA algorithm will have a large gap with the system expectation value, which wastes the system computing resources to a large extent. The simulation results demonstrate that the BER performance of low power users will be evidently improved with a reasonable power allocation algorithm in the strong turbulent environment at the limited BER expense of high power users.

In addition, the results of average BER with two 2-user paired NOMA scenarios are presented in Table 3. It can be told that the proposed GSPA algorithm obviously outperforms the FPA and the DFPA with the less average BER in any scenario. Furthermore, the optimization efficiency of the proposed GSPA for users in strong turbulent environment is better than that of users in the weak turbulent environment.

The performance of the proposed GSPA algorithm is further accessed in the 3-user paired UWOC-NOMA system. The results are shown in Fig. 9. It can be observed that compared to that of the proposed GSPA algorithm, the BER gap of User 1 and User 3 with the FPA and the DFPA algorithms is even large. This phenomenon is mainly attributed to the following two reasons. First, the traditional power allocation algorithm, both the FPA and the DFPA algorithms, prioritizes ascertaining the power allocation coefficients for the two users with the greatest channel quality difference, which exacerbates the unfairness of power allocation for the multi-user paired NOMA systems. Second, the FPA and the DFPA algorithms ignore the fading characteristic of underwater optical channel, and the light intensity scintillation caused by turbulence, which has a significant impact on the BER of NOMA users. The DSPA algorithm effectively reduces the BER gap between NOMA paired users. According to the comparison in Fig. 9(a)-(c), it can be seen that although the

TABLE 3. Average BER of three schemes with two 2-user paired NOMA scenarios.

P_t=27.5dBm		$\sigma^2_{sci}=0.1$	$\sigma^2_{sci}=0.5$	$\sigma^2_{sci}=1.0$
$S_{1,2}$	FPA	8.73×10^{-5}	3.62×10^{-3}	3.49×10^{-2}
	DFPA	7.61×10^{-5}	3.01×10^{-3}	3.67×10^{-2}
	GSPA	9.60×10^{-6}	1.81×10^{-3}	5.87×10^{-3}
$S_{1,3}$	FPA	1.05×10^{-4}	1.71×10^{-2}	1.10×10^{-1}
	DFPA	1.53×10^{-4}	1.54×10^{-2}	1.14×10^{-1}
	GSPA	2.05×10^{-5}	2.61×10^{-3}	8.28×10^{-3}

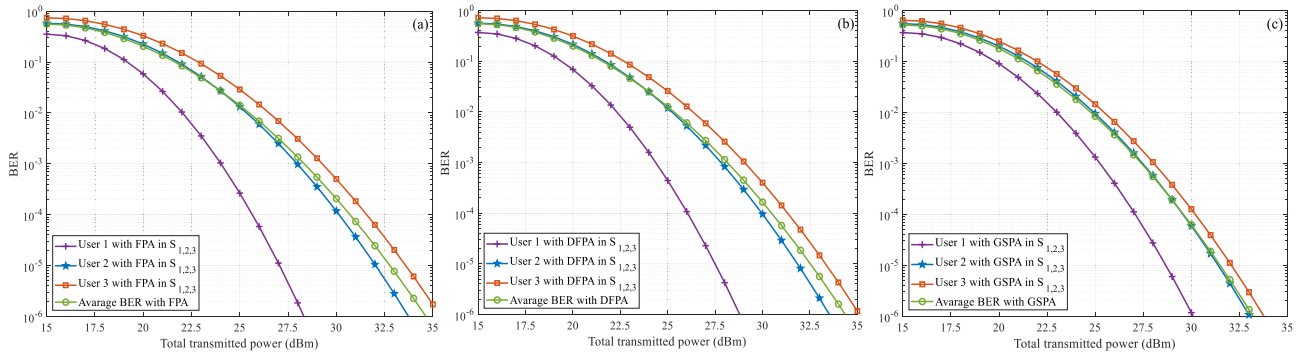

FIGURE 9. BER for the 3-user paired UWOC-NOMA scenario for (a)FPA, (b)DFPA, (c)GSPA.

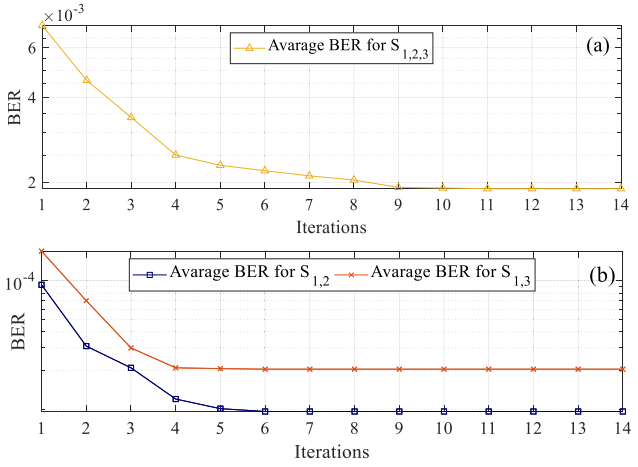

FIGURE 10. Convergence behavior of the proposed GSPA algorithm for (a) 3-user paired scenario, (b) 2-user paired scenario.

DSPA algorithm sacrifices the BER performance of User 1, the DSPA algorithm can still get the lowest average BER in the same transmitted power region.

The convergence behaviour of the proposed GSPA algorithm with respect to different UWOC-NOMA scenarios is illustrated in Fig. 10, where the proposed GSPA algorithm requires 10, 5 and 6 iterations to obtain the minimal BER for $S_{1,2,3}$, $S_{1,2}$ and $S_{1,3}$, respectively. It can be conducted that the convergence rate of this power allocation algorithm is principally related to the number of paired users in a single NOMA group, and it is basically independent of the channel quality difference between NOMA paired users.

VI. CONCLUSION

This paper analyzes the decoding error caused by the self-interference of the NOMA paired group in the oceanic turbulence channel. An alternating composite phase shift coding scheme based on constellation optimization is proposed for the UWOC-NOMA system, which eliminates the interference of the high power users to the low-power users in the NOMA paired group, and thus reduces the BER of NOMA users. Moreover, a power allocation algorithm based on BER optimization is presented for the proposed UWOC-NOMA system. Therein, the optimization problem is proved to be strictly convex and the solutions are obtained by our GSPA algorithm. The simulation results indicate that the proposed algorithm can obtain desirable average BER performance with relatively faster convergence.

APPENDIX A

The Taylor series expansion of (2) can be expressed as

$$\begin{aligned} f(I) &= \frac{\delta\beta}{\alpha}\left(\frac{I}{\alpha}\right)^{\beta-1}\left\{\exp\left(-\left(\frac{I}{\alpha}\right)^{\beta}\right)\right\}^{\delta-1} \\ &= \frac{\delta\beta}{\alpha}\left(\frac{I}{\alpha}\right)^{\beta-1}\left[\sum_{n=0}^{\infty}\left\{1-\left(\frac{I}{\alpha}\right)^{\delta\beta-\beta}+\frac{1}{2}\left(\frac{I}{\alpha}\right)^{2(\delta\beta-\beta)}\right.\right. \\ &\quad \left.\left.-\frac{1}{6}\left(\frac{I}{\alpha}\right)^{3(\delta\beta-\beta)}+\frac{1}{24}\left(\frac{I}{\alpha}\right)^{4(\delta\beta-\beta)}+\ldots\right\}\right] \end{aligned} \tag{A.1}$$

In conjunction with (3)-(6), (A.1) can be given as the following expressions with Lagrange approximation

$$f(I)\approx\frac{\delta\beta}{\alpha}\left(\frac{I}{\alpha}\right)^{\beta-1}\left[\sum_{n=0}^{\infty}1-\left(\frac{I}{\alpha}\right)^{\delta\beta-\beta}+\frac{1}{2}\left(\frac{I}{\alpha}\right)^{2(\delta\beta-\beta)}\right] \tag{A.2}$$

According to the BER judgment region in Fig. 3(b), the BER of user 1 can be obtained as

$$\begin{aligned} P_{\mathrm{U1,O}} &= \frac{1}{2}\int_0^{\infty} Q\left(2\frac{t'_{1,1}+t'_{2,1}}{B}I\right) \\ &\quad + Q\left(2\frac{t'_{1,1}-t'_{2,1}}{B}I\right) f\left(I\right)\mathrm{d}I \\ &= \frac{1}{2}\int_0^{\infty} Q\left(2\frac{t'_{1,1}+t'_{2,1}}{B}I\right) f\left(I\right)\mathrm{d}I \\ &\quad + \frac{1}{2}\int_0^{\infty} Q\left(2\frac{t'_{1,1}-t'_{2,1}}{B}I\right) f\left(I\right)\mathrm{d}I \end{aligned} \tag{A.3}$$

Let $\rho_{a_1} = 2\left(t'_{1,1}+t'_{2,1}\right)\Big/B$, and then, the first term of the integral in (A.3) can be denoted as

$$\begin{aligned} &\Theta\left(\rho_{a_1}\right) \\ &= \int_0^{\infty} Q\left(\rho_{a_1} I\right) f\left(I\right)\mathrm{d}I \\ &= \left(1+\frac{\delta\beta}{\alpha}\right)\left(1-\exp\left(\left(\frac{\delta\beta-\beta}{\rho_{a_1}}\right)^2\right)Q\left(\frac{\delta\beta-\beta}{\rho_{a_1}}\right)\right) \\ &\quad - \frac{2\delta\beta}{\alpha} + \frac{2\delta\beta^2}{\alpha}\frac{1}{\sqrt{\pi}\rho_{a_1}} \\ &\quad + \frac{\delta\beta^2}{\alpha}\left(\left(\frac{1}{\beta}\right)^2 - \frac{1}{2}\left(\frac{1}{\rho_{a_1}}\right)^2\right) \\ &\quad \times \exp\left(\left(\frac{\delta\beta-\beta}{\rho_{a_1}}\right)^2\right)Q\left(\frac{\delta\beta-\beta}{\rho_{a_1}}\right) \end{aligned} \tag{A.4}$$

Simplifying (A.4), we can get the following expression

$$\begin{aligned} \Theta\left(\rho_{a_1}\right) &= \int_0^{\infty} Q\left(\rho_{a_1} I\right) f\left(I\right)\mathrm{d}I \\ &= 1 - \frac{\delta\beta}{\alpha} + \frac{2\delta\beta^2}{\alpha\sqrt{\pi}\rho_{a_1}} \\ &\quad + \left(\frac{\delta\beta}{\alpha} - \left(\frac{\delta\beta-\beta}{\rho_{a_1}}\right)^2 - 1\right) \\ &\quad \times \exp\left(\left(\frac{\delta\beta-\beta}{\rho_{a_1}}\right)^2\right)Q\left(\frac{\delta\beta-\beta}{\rho_{a_1}}\right) \end{aligned} \tag{A.5}$$

The second integral term in (A.3) can be obtained in the same way.

APPENDIX B

According to the judgment boundary of the constellation diagram, the misjudged region for b_1, or b_2 can be obtained from the position relationship of constellation points $(a_1, a_2) = (0,0)$ or $(0,1)$.

The BER of b_1 can be expressed as

$$\begin{aligned} P_{b_1} &= \frac{1}{2}\left(P_{b_1=0} + P_{b_1=1}\right) \\ &= \frac{1}{2}\left(P_{b_1=0|(a_1,a_2)=(0,0)} + P_{b_1=0|(a_1,a_2)=(0,1)}\right. \\ &\quad \left. + P_{b_1=1|(a_1,a_2)=(0,0)} + P_{b_1=1|(a_1,a_2)=(0,1)}\right) \end{aligned} \tag{B.1}$$

The BER of each constellation point can be calculated by (B.2)- (B.5)

$$\begin{aligned} &P_{b_1=0|(a_1,a_2)=(0,0)} \\ &= \frac{1}{4}\left\{\Theta\left(\frac{t_{2,2}}{\sqrt{N_2/2}}\right)\right. \\ &\quad + \sum_{i=2}^{5}(-1)^{i+1}\,\Theta\left(\frac{it_{2,1}-\left(2\left(-1\right)^i+3\right)t_{2,2}}{\sqrt{N_2/2}}\right) \\ &\quad \left. + \sum_{j=1}^{3}(-1)^{j}\,\Theta\left(\frac{jt_{2,1}+\left(2\left(-1\right)^j+3\right)t_{2,2}}{\sqrt{N_2/2}}\right)\right\} \end{aligned} \tag{B.2}$$

$$\begin{aligned} &P_{b_1=0|(a_1,a_2)=(0,1)} \\ &= \frac{1}{4}\left\{\Theta\left(\frac{t_{2,2}}{\sqrt{N_2/2}}\right) + \left[\sum_{i=1}^{2}\sum_{j=i}^{2+i-1}(-1)^{i+1}\,\Theta\right.\right. \\ &\quad \times \left(\frac{\left(2j-1\right)t_{2,1}-\left(-1\right)^i t_{2,2}}{\sqrt{N_2/2}}\right) \\ &\quad \left.\left. + (-1)^i\,\Theta\left(\frac{\left(2j-2\right)t_{2,1}-\left(-1\right)^i 5t_{2,2}}{\sqrt{N_2/2}}\right)\right] \right. \\ &\quad \left. + \sum_{m=1}^{2}(-1)^{m+1}\,\Theta\left(\frac{\left(2m-1\right)t_{2,1}+\left(-1\right)^m t_{2,2}}{\sqrt{N_2/2}}\right)\right\} \end{aligned} \tag{B.3}$$

$$\begin{aligned} &P_{b_1=1|(a_1,a_2)=(0,0)} \\ &= \frac{1}{4}\left\{2\sum_{l=1}^{2}\Theta\left(\frac{\left(2l-1\right)t_{2,2}}{\sqrt{N_2/2}}\right)\right. \\ &\quad + \sum_{i=1}^{2}\sum_{j=1}^{2}\Theta\left(\frac{2t_{2,1}-\left(-1\right)^{i+j}\left(2i-1\right)t_{2,2}}{\sqrt{N_2/2}}\right) \\ &\quad \left. + \sum_{m=1}^{2}\Theta\left(\frac{4t_{2,1}-\left(2m-1\right)t_{2,2}}{\sqrt{N_2/2}}\right)\right\} \end{aligned} \tag{B.4}$$

$$\begin{aligned} &P_{b_1=1|(a_1,a_2)=(0,1)} \\ &= \frac{1}{4}\left\{\left[\sum_{i=1}^{2}\Theta\left(\frac{2t_{2,1}+\left(5-2i\right)t_{2,2}}{\sqrt{N_2/2}}\right)\right.\right. \\ &\quad \left.\left. -\Theta\left(\frac{4t_{2,1}+\left(2i-1\right)t_{2,2}}{\sqrt{N_2/2}}\right)\right. \end{aligned}$$

$$-\Theta\left(\frac{2t_{2,1}+(2i-1)\,t_{2,2}}{\sqrt{N_2/2}}\right)\Bigg]+2\sum_{j=1}^{2}\Theta\left(\frac{(5-2j)\,t_{2,2}}{\sqrt{N_2/2}}\right)\Bigg\} \tag{B.5}$$

APPENDIX C

According to **Appendix A** and (18), let $\kappa=\sqrt{P_t h_2/2n_2}$, and then, the first and second order derivatives of P_{U2} with respect to a_1 can be expressed by (C.1)- (C.5), respectively.

$$\begin{aligned}\frac{\partial P_{\mathrm{U2}}}{\partial a_1}&=\frac{\delta\beta^2}{\alpha\sqrt{\pi}}\frac{\sqrt{2}\kappa}{2}\frac{1}{2}\Bigg[\frac{1}{\sqrt{a_1}}\Bigg(\left(\frac{4t_1t_2}{\left(4t_1^2-t_2^2\right)^2}+\frac{4t_1^2+t_2^2}{\left(4t_1^2-t_2^2\right)^2}\right)\\&\quad-\left(\frac{2t_1t_2}{\left(t_1^2-t_2^2\right)^2}-\frac{t_1^2+t_2^2}{\left(t_1^2-t_2^2\right)^2}\right)\Bigg)\Bigg]\\&\quad+\frac{\delta\beta^2}{\alpha\sqrt{\pi}}\frac{\sqrt{2}\kappa}{2}\frac{1}{\sqrt{a_1}}\left[2\frac{(2t_1+t_2)^2}{\left(4t_1^2-t_2^2\right)^2}-\frac{(t_1+t_2)^2}{\left(t_1^2-t_2^2\right)^2}\right]\\&\quad\times\left(1-Q\left(\frac{\delta\beta-\beta}{2t_2+t_1}\right)\right)\\&\quad+\frac{\delta\beta^2}{\alpha\sqrt{\pi}}\frac{\sqrt{2}\kappa}{2}\frac{1}{2}\frac{1}{\sqrt{a_1}}\exp\left(3t_1^2-6t_1t_2\right)\end{aligned} \tag{C.1}$$

$$\begin{aligned}\frac{\partial^2 P_{\mathrm{U2}}}{\partial a_1^2}&=-\frac{\delta\beta^2}{\alpha\sqrt{\pi}}\frac{\sqrt{2}\kappa^2}{8}\frac{1}{a_1}\left(\frac{-8t_1}{\left(2t_1^2-t_2^2\right)^3}+\frac{-2}{(t_1+t_2)^3}\right)\\&\quad-\frac{\delta\beta^2}{\alpha\sqrt{\pi}}\frac{\sqrt{2}\kappa}{8}\frac{1}{a_1\sqrt{a_1}}\left(\frac{1}{\left(2t_1^2-t_2^2\right)^2}+\frac{1}{(t_1+t_2)^2}\right)\\&\quad-\frac{\delta\beta^2}{\alpha\sqrt{\pi}}\frac{\sqrt{2}\kappa}{4}\frac{1}{a_1\sqrt{a_1}}\left[2\frac{1}{(2t_1-t_2)^2}-\frac{1}{(t_1-t_2)^2}\right]\\&\quad\times\left[1-Q\left(\frac{\delta\beta-\beta}{2t_2+t_1}\right)\right]\\&\quad+\frac{\delta\beta^2}{\alpha\sqrt{\pi}}\frac{\sqrt{2}\kappa^2}{4}\frac{1}{a_1}\left(\frac{-16t_1}{\left(2t_1^2-t_2^2\right)^3}+\frac{-2}{(t_1+t_2)^3}\right)\\&\quad\times\left[1-Q\left(\frac{\delta\beta-\beta}{2t_2+t_1}\right)\right]\\&\quad+\frac{\delta\beta^2}{\alpha\sqrt{\pi}}\frac{\sqrt{2}\kappa^2}{2}\frac{1}{a_1}\left[2\frac{1}{(2t_1-t_2)^2}-\frac{1}{(t_1-t_2)^2}\right]\\&\quad\times\exp\left(\frac{\delta\beta-\beta}{2t_2+t_1}\right)\\&\quad+\frac{\delta\beta^2}{\alpha\sqrt{\pi}}\frac{\sqrt{2}\kappa^2}{2}\frac{1}{2}\frac{1}{a_1}\left(6t_1-6t_2\right)\exp\left(3t_1^2-6t_1t_2\right)\\&\quad-\frac{\delta\beta^2}{\alpha\sqrt{\pi}}\frac{\sqrt{2}\kappa}{2}\frac{1}{2}\frac{1}{a_1\sqrt{a_1}}\exp\left(3t_1^2-6t_1t_2\right)\end{aligned} \tag{C.2}$$

$$\begin{aligned}\frac{\partial^2 P_{\mathrm{U2}}}{\partial a_1\partial a_2}&=-\frac{\delta\beta^2}{\alpha\sqrt{\pi}}\frac{\sqrt{2}\kappa^2}{8}\frac{1}{\sqrt{a_1a_2}}\left(\frac{-4t_2}{\left(2t_1^2-t_2^2\right)^3}+\frac{-2}{(t_1+t_2)^3}\right)\\&\quad+\frac{\delta\beta^2}{\alpha\sqrt{\pi}}\frac{\sqrt{2}\kappa^2}{2}\frac{1}{\sqrt{a_1a_2}}\left(\frac{-8t_2}{\left(2t_1^2-t_2^2\right)^3}+\frac{-2}{(t_1+t_2)^3}\right)\\&\quad\times\left[1-Q\left(\frac{\delta\beta-\beta}{2t_2+t_1}\right)\right]\\&\quad-\frac{\delta\beta^2}{\alpha\sqrt{\pi}}\frac{\sqrt{2}\kappa^2}{2}\frac{1}{\sqrt{a_1a_2}}\left[2\frac{1}{(2t_1-t_2)^2}-\frac{1}{(t_1-t_2)^2}\right]\\&\quad\times\exp\left(\frac{\delta\beta-\beta}{2t_2+t_1}\right)\\&\quad+\frac{\delta\beta^2}{\alpha\sqrt{\pi}}\frac{\sqrt{2}\kappa^2}{2}\frac{1}{2}\frac{6t_1}{\sqrt{a_1a_2}}\exp\left(3t_1^2-6t_1t_2\right)\end{aligned} \tag{C.3}$$

$$\begin{aligned}\frac{\partial P_{\mathrm{U2}}}{\partial a_2}&=\frac{\partial\Theta(t_2)}{\partial a_2}+\frac{1}{2}\Bigg\{\frac{\partial a_1}{\partial a_2}\frac{\sqrt{a_2}}{2\sqrt{a_1}}\\&\quad\times\left(\frac{\partial\Theta(2t_1+t_2)}{\partial a_1}-\frac{\partial\Theta(2t_1-t_2)}{\partial a_1}\right)\\&\quad-\frac{\partial a_1}{\partial a_2}\frac{\sqrt{a_2}}{\sqrt{a_1}}\left(\frac{\partial\Theta(t_1+t_2)}{\partial a_1}-\frac{\partial\Theta(t_1-t_2)}{\partial a_1}\right)\Bigg\}\end{aligned} \tag{C.4}$$

$$\begin{aligned}\frac{\partial^2 P_{\mathrm{U2}}}{\partial a_2^2}&=\frac{\partial^2\Theta(t_2)}{\partial a_2^2}+\frac{1}{2}\Bigg\{\frac{\partial a_1^2}{\partial a_2^2}\frac{a_2}{4a_1}\\&\quad\times\left(\frac{\partial^2\Theta_2(2t_1+t)}{\partial a_1^2}-\frac{\partial\Theta(2t_1-t_2)}{\partial a_1^2}\right)\\&\quad-\frac{\partial a_1^2}{\partial a_2^2}\frac{a_2}{a_1}\left(\frac{\partial\Theta(t_1+t_2)}{\partial a_1^2}-\frac{\partial\Theta(t_1-t_2)}{\partial a_1^2}\right)\Bigg\}\end{aligned} \tag{C.5}$$

where $Q(\cdot)$ denotes the standard normal distribution function, i.e., $0<Q(\cdot)<1$. Without loss of generality, this paper simultaneously takes into account the weak, medium and strong turbulent channels, thus proves that $(\delta\beta-\beta)^2\exp(\delta\beta-\beta)-\left(1/(\delta\beta-\beta)\right)\left(\exp(\delta\beta-\beta)^2\right)Q((\delta\beta-\beta))>0$ and $\partial\Theta(t_2)/\partial a_2<0$, $\partial^2\Theta(t_2)/\partial a_2^2<0$. In addition to that, according to the power distribution principle of NOMA,

$a_1>a_2$, then $\partial P_{\mathrm{U2}}/\partial a_1>0>\partial P_{\mathrm{U2}}/\partial a_2$, $\partial^2 P_{\mathrm{U2}}/\partial^2 a_1>0$ and $\partial^2 P_{\mathrm{U2}}/\partial a_1^2>\partial^2 P_{\mathrm{U2}}/\partial a_1\partial a_2>\partial^2 P_{\mathrm{U2}}/\partial a_2^2$, can be proved. Therefore, we can conduct the followings

$$\det(\mathbf{H}_2)=-\left(\frac{\partial P_{\mathrm{U2}}}{\partial a_1}\right)^2<0, \tag{C.6}$$

$$\det(\mathbf{H})=\frac{\partial P_{\mathrm{U2}}}{\partial a_1}\frac{\partial P_{\mathrm{U2}}}{\partial a_1}\frac{\partial^2 P_{\mathrm{U2}}}{\partial a_1^2}-\frac{\partial P_{\mathrm{U2}}}{\partial a_1}\frac{\partial^2 P_{\mathrm{U2}}}{\partial a_1\partial a_2}\frac{\partial P_{\mathrm{U2}}}{\partial a_2}$$

$$+\frac{\partial P_{U2}}{\partial a_2}\frac{\partial^2 P_{U2}}{\partial a_1^2}\frac{\partial P_{U2}}{\partial a_2}-\frac{\partial P_{U2}}{\partial a_2}\frac{\partial P_{U2}}{\partial a_1}\frac{\partial^2 P_{U2}}{\partial a_1 \partial a_2}. \tag{C.7}$$

It can be conducted from (C.6) and (C.7) that the optimization problem in (19) is strictly convex with respect to a_1, and the local optimal solution of the strictly convex problem is the global optimal solution.

REFERENCES

[1] H. Kaushal and G. Kaddoum, "Underwater optical wireless communication," *IEEE Access*, vol. 4, pp. 1518–1547, 2016.

[2] S. Jaruwatanadilok, "Underwater wireless optical communication channel modeling and performance evaluation using vector radiative transfer theory," *IEEE J. Sel. Areas Commun.*, vol. 26, no. 9, pp. 1620–1627, Dec. 2008.

[3] T. Komine and M. Nakagawa, "Fundamental analysis for visible-light communication system using LED lights," *IEEE Trans. Consum. Electron.*, vol. 50, no. 1, pp. 100–107, Feb. 2004.

[4] P. H. Pathak, X. Feng, P. Hu, and P. Mohapatra, "Visible light communication, networking, and sensing: A survey, potential and challenges," *IEEE Commun. Surveys Tuts.*, vol. 17, no. 4, pp. 2047–2077, 4th Quart., 2015.

[5] D. Karunatilaka, F. Zafar, V. Kalavally, and R. Parthiban, "LED based indoor visible light communications: State of the art," *IEEE Commun. Surveys Tuts.*, vol. 17, no. 3, pp. 1649–1678, 3rd Quart., 2015.

[6] M. Jouhari, K. Ibrahimi, H. Tembine, and J. Ben-Othman, "Underwater wireless sensor networks: A survey on enabling technologies, localization protocols, and Internet of Underwater Things," *IEEE Access*, vol. 7, pp. 96879–96899, 2019.

[7] Y. Liang, H. Yin, L. Jing, X. Ji, and J. Wang, "Performance analysis of relay-aided NOMA optical wireless communication system in underwater turbulence environment," *Remote Sens.*, vol. 14, no. 16, p. 3894, Aug. 2022.

[8] R. Jiang, C. Sun, X. Tang, L. Zhang, H. Wang, and A. Zhang, "Joint user-subcarrier pairing and power allocation for uplink ACO-OFDM-NOMA underwater visible light communication systems," *J. Lightw. Technol.*, vol. 39, no. 7, pp. 1997–2007, Apr. 1, 2021.

[9] D. Chen, Y. Wang, J. Jin, H. Lu, and J. Wang, "An experimental study of NOMA in underwater visible light communication system," *Opt. Commun.*, vol. 475, Nov. 2020, Art. no. 126199.

[10] M. Elamassie, L. Bariah, M. Uysal, S. Muhaidat, and P. C. Sofotasios, "Capacity analysis of NOMA-enabled underwater VLC networks," *IEEE Access*, vol. 9, pp. 153305–153315, 2021.

[11] Y. Tsuzuki, S. Shimamoto, and Z. Pan, "Evaluations of SIC by power difference in IM-NOMA," in *Proc. Wireless Days (WD)*, Jun. 2021, pp. 1–5.

[12] S. Herfiah and Iskandar, "Effect of imperfect SIC in non-orthogonal multiple access (NOMA) over Rayleigh fading channels," in *Proc. 7th Int. Conf. Wireless Telematics (ICWT)*, Aug. 2021, pp. 1–4.

[13] Q. Li, T. Shang, T. Tang, and Z. Dong, "Optimal power allocation scheme based on multi-factor control in indoor NOMA-VLC systems," *IEEE Access*, vol. 7, pp. 82878–82887, 2019.

[14] L. Bariah, M. Elamassie, S. Muhaidat, P. C. Sofotasios, and M. Uysal, "Non-orthogonal multiple access-based underwater VLC systems in the presence of turbulence," *IEEE Photon. J.*, vol. 14, no. 1, pp. 1–7, Feb. 2022.

[15] L. Zhang, Y. Chen, K. Zhang, J. Quan, Z. Li, and Y. Dong, "On performance of multiuser underwater wireless optical communication systems," in *Proc. Int. Conf. Comput., Netw. Commun. (ICNC)*, Feb. 2020, pp. 1042–1046.

[16] A. Kumar, S. Al-Kuwari, D. N. K. Jayakody, and R. Alkanhel, "Security performance analysis of a NOMA-assisted underwater VLC system under imprecise channel estimations," *IEEE Access*, vol. 10, pp. 117021–117032, 2022.

[17] S. Afifah, L. Marlina, C.-C. Chen, Y.-L. Liu, S.-K. Liaw, and C.-H. Yeh, "Impact of artificial seawater and turbulence factors on underwater optical wireless communication," in *Proc. 30th Wireless Opt. Commun. Conf. (WOCC)*, Oct. 2021, pp. 110–114.

[18] Y. Weng, Y. Guo, O. Alkhazragi, T. K. Ng, J.-H. Guo, and B. S. Ooi, "Impact of turbulent-flow-induced scintillation on deep-ocean wireless optical communication," *J. Lightw. Technol.*, vol. 37, no. 19, pp. 5083–5090, Oct. 1, 2019.

[19] H. Jiang, H. Qiu, N. He, W. Popoola, Z. Ahmad, and S. Rajbhandari, "Performance of spatial diversity DCO-OFDM in a weak turbulence underwater visible light communication channel," *J. Lightw. Technol.*, vol. 38, no. 8, pp. 2271–2277, Apr. 15, 2020.

[20] A. Jurado-Navas, N. G. Serrato, J. Garrido-Balsells, and M. Castillo-Vázquez, "Error probability analysis of OOK and variable weight MPPM coding schemes for underwater optical communication systems affected by salinity turbulence," *OSA Continuum*, vol. 1, no. 4, pp. 1131–1143, 2018.

[21] L. Cang, H.-K. Zhao, H. Liu, W.-L. Ji, Y.-B. Wan, K. Zhang, and G.-X. Zheng, "Terahertz MIMO communication performance analysis in exponentiated Weibull turbulence with pointing errors," *Appl. Opt.*, vol. 60, no. 24, pp. 7314–7325, 2021.

[22] X. Ji, H. Yin, L. Jing, Y. Liang, and J. Wang, "Modeling and performance analysis of oblique underwater optical communication links considering turbulence effects based on seawater depth layering," *Opt. Exp.*, vol. 30, no. 11, pp. 18874–18888, 2022.

[23] Z. Rahman, S. M. Zafaruddin, and V. K. Chaubey, "Performance analysis of optical wireless communications with aperture averaging over exponentiated Weibull turbulence with pointing errors," *Results Opt.*, vol. 5, Dec. 2021, Art. no. 100171.

[24] M. V. Jamali, A. Mirani, A. Parsay, B. Abolhassani, P. Nabavi, A. Chizari, P. Khorramshahi, S. Abdollahramezani, and J. A. Salehi, "Statistical studies of fading in underwater wireless optical channels in the presence of air bubble, temperature, and salinity random variations," *IEEE Trans. Commun.*, vol. 66, no. 10, pp. 4706–4723, Oct. 2018.

[25] A. Celik, N. Saeed, T. Y. Al-Naffouri, and M. -S. Alouini, "Modeling and performance analysis of multihop underwater optical wireless sensor networks," in *Proc. IEEE Wireless Commun. Netw. Conf. (WCNC)*, Apr. 2018, pp. 1–6.

[26] J. Zhang, G. Gao, B. Wang, X. Guan, L. Yin, J. Chen, and B. Luo, "Background noise resistant underwater wireless optical communication using Faraday atomic line laser and filter," *J. Lightw. Technol.*, vol. 40, no. 1, pp. 63–73, Jan. 2022.

[27] K. Cho and D. Yoon, "On the general BER expression of one- and two-dimensional amplitude modulations," *IEEE Trans. Commun.*, vol. 50, no. 7, pp. 1074–1080, Jul. 2002.

YANJUN LIANG received the B.S. degree in electronic information engineering from Chang'an University, China, in 2015, and the M.S. degree in electronics and communication engineering from Hainan University, China, in 2019. He is currently pursuing the Ph.D. degree in communication and information system with the Dalian University of Technology. His research interest includes the new multiple access technologies in underwater optical wireless communication.

HONGXI YIN received the B.S. degree from Shandong University, in 1982, the M.E. degree from the Harbin Institute of Technology, in 1988, and the Ph.D. degree from Zhongshan University, China, in 1998.

He was a Postdoctoral Researcher and an Associate Professor with Peking University, China, from 1998 to 2008, and a Research Fellow with the University of Southampton, U.K., from 2005 to 2007. He is currently a Professor with the School of Information and Communication Engineering, Dalian University of Technology. He has authored or coauthored more than 200 journal articles and conference papers in the areas of optical communication systems and networks and held 15 Chinese national invention patents. His research interests include advanced optical fiber communication systems and networks, satellite light communication and networking, underwater optical wireless communication and sensor networks, and photonic reservoir computing.

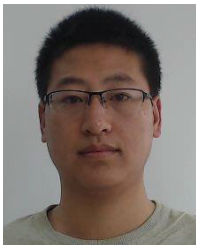

LIANYOU JING (Member, IEEE) received the B.S., M.S., and Ph.D. degrees in electronic and communication engineering from the School of Marine Science and Technology, Northwestern Polytechnical University, Shaanxi, China, in 2010, 2013, and 2017, respectively. He is currently a Faculty Member with the School of Information and Communication Engineering, Dalian University of Technology. His current research interest includes underwater acoustic communications.

XIUYANG JI received the B.Eng. degree in communication engineering from the Dalian University of Technology (DLUT), China, in 2016, where he is currently pursuing the Ph.D. degree in communication engineering with the Laboratory of Optical Communications and Photonic Technology. His research interests include underwater optical wireless communication and underwater channel modeling.

JIANYING WANG received the B.S. degree in electronic information science and technology and the M.S. degree in communication and information system from Xinjiang University, Ürümqi, China, in 2003 and 2006, respectively. She is currently pursuing the Ph.D. degree in signal and information processing with the Laboratory of Optical Communications and Photonic Technology, Dalian University of Technology, Dalian, China. Her research interests include underwater wireless optical MIMO technology and communication systems.